

Chapter II

Analysis of Scattered Waves from Two Layers of Tree Trunk

2.1. Introduction

Pine (*Pinus Merkusii*) is the important plant in Indonesia, especially Java and Sumatra islands as a source of turpentine or volatile oil (Coppen *et al.* 1993), see figure 1.2. Turpentine is distilled from the pine resin. Traditionally, turpentine has been employed as a solvent or cleaning agent for paints and varnishes. Most turpentine nowadays is used as a source of chemical isolations that are then converted into a wide range of products. Many of these, including the biggest single turpentine derivative and synthetic pine oil, are employed for fragrance and flavour use, although there are also many important non-aromatic applications such as polyterpene resins. Pine oil is used in disinfectants, cleaning agents and other products having a pine odour (FAO 1995). Turpentine is obtained via tapping of living pine trees (whether natural stands or plantations). Pine is multi purposes plant, if its tapped then the felled trees provide income from sale of the logs for timber or pulp.

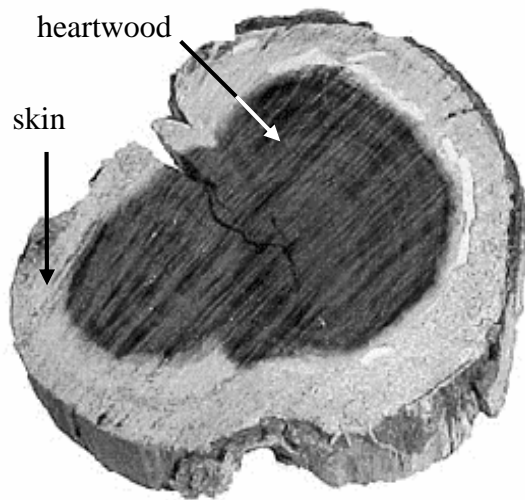
Indonesia is large archipelago that consists of more than 1,700 large islands with land territory covers approximately 1.9 million square kilometres. It is very difficult to estimate age or volume of pine using conventional techniques that spent much time and cost to collect its ground data. Recently, remote sensing technology has been an efficient and helpful tool to monitor forest and plantation in a large area. The main problem in monitoring tropical areas, as Indonesia, is cloudy conditions. The best instrument to monitor these areas is synthetic aperture radar (SAR), as it works effectively in spite of cloudy conditions. However, SAR data are not easily interpreted due to the complex relations of the radar backscattering mechanisms between microwaves and pine trunk. In this study, the author attempts to find the

relationships between the radar backscattering coefficients and the diameter of pine trunk that are found in Indonesian forests and plantations.

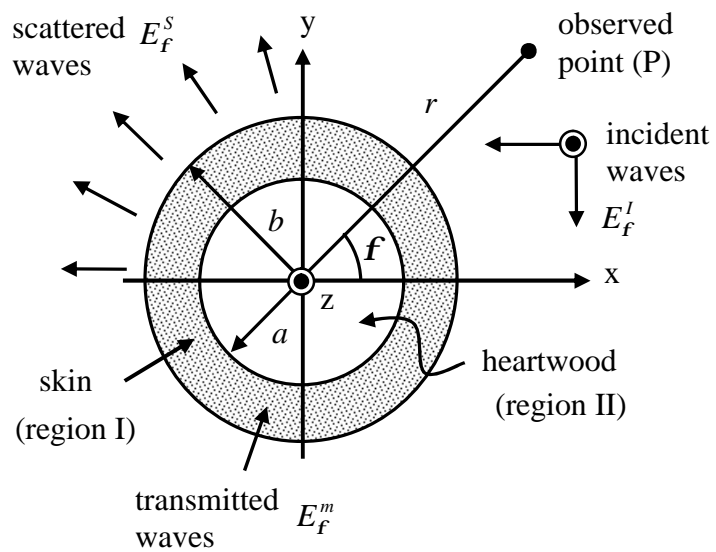
In this study, a simple analysis of scattered wave from a pine trunk was done in order to estimate the relationship between diameter of tree trunk and its backscattering coefficients \mathbf{s}^o . In section 2.2, the modelling and formulation of scattering problems on pine are discussed. In section 2.3, the simulation of transverse electric (TE) wave propagation is done using Finite Difference Time Domain (FDTD) method. In section 2.4, the analytical results are verified by comparing them with the simulated results. The application of this research will be introduced in section 2.5. Finally, conclusions are given in section 2.6.

2.2. Analysis

Figure 2.1(a) shows photograph of pine trunk that found at west Java, Indonesia. Actually, its tree trunk is composed of two media; skin and heartwood. In this study, the analysis of scattered wave from its tree trunk is discussed in order to investigate the correlation of backscattering coefficient \mathbf{s}^o and the diameter of tree trunk. This scattering problem in its tree trunk is analysed using mode expansion method (Tetuko *et al.* 2001). The two-dimensional model of tree trunk is shown in figure 2.1(b). Two layers of media compose this model of a tree trunk with infinite length in z-axis. The radii of heartwood and skin layer are a and b , respectively. Several trunks of pine trees that were found around the study area, were measured and the results showed that approximately each component had relations $a=0.5b$. The properties of skin are determined by complex dielectric constant \mathbf{e}_r and complex permeability \mathbf{m} . The dielectric constant \mathbf{e}_r of several skin medium of pine samples were measured experimentally by the author using dielectric probe kit HP85070B and the result was $3.1-j0.4$ (see figure 1.8 (a)). The water content of heartwood is high, consequently, heartwood was assumed to be an infinite length of perfect conductor or electromagnetic fields



(a) Photograph of a cross section of pine (*Pinus merkusii*) trunk.



(b) Geometry of scattered waves from a pine trunk.

Figure 2.1. Photograph and geometry of the analysis.

in heartwood is zero. Here, incident wave is assumed as a plane wave that has transverse electric (TE) mode and incident angle \mathbf{f} with respect to direction of observed point P from origin of coordinate. This wave propagation is $-x$ direction. Based on this figure and Appendix E, the z component of the magnetic fields in free space and skin are determined as

$$\text{Incident wave} \quad H_z^I = H_o^I \sum_{m=0}^{\infty} U_m J_m(k_o r) j^m \cos m\mathbf{f} \quad (r > b) \quad (2.1)$$

$$\text{Scattered wave} \quad H_z^S = H_o^I \sum_{m=0}^{\infty} b_m H_m^{(2)}(k_o r) \cos m\mathbf{f} \quad (r > b) \quad (2.2)$$

$$\text{Transmitted wave} \quad H_z^m = H_o^I \sum_{m=0}^{\infty} \{a_m J_m(kr) + a'_m N_m(kr)\} \cos m\mathbf{f} \quad (a \leq r \leq b) \quad (2.3)$$

Where the wave number of skin is $k = k_o \sqrt{\mathbf{m}, \mathbf{e}_r}$ and k_o is wave number in free space. a_m to b_m are amplitude coefficients. H_o^I is initial amplitude of incident magnetic field. J_m , N_m , and $H_m^{(2)}$ are m -th order of Bessel function, Neumann function, and 2nd kind of Hankel function. Where

$$U_m = \begin{cases} 1 & (m = 0) \\ 2 & (m = 1, 2, 3, \dots) \end{cases} \quad (2.4)$$

By substituting (2.1) to (2.3) into Maxwell's equations below

$$\nabla \times \mathbf{H} = \mathbf{e} \frac{\partial \mathbf{E}}{\partial t} \quad (2.5)$$

the electric field of each medium was derived as

$$E_f^I = -\frac{k_o H_o^I}{j\omega \mathbf{e}_o} \sum_{m=0}^{\infty} U_m J'_m(k_o r) j^m \cos m\mathbf{f} \quad (r > b) \quad (2.6)$$

$$E_f^S = -\frac{k_o H_o^I}{j\omega \mathbf{e}_o} \sum_{m=0}^{\infty} b_m H_m^{(2)'}(k_o r) \cos m\mathbf{f} \quad (r > b) \quad (2.7)$$

$$E_f^m = -\frac{k H_o^I}{j\omega \mathbf{e}} \sum_{m=0}^{\infty} \{a_m J'_m(kr) + a'_m N'_m(kr)\} \cos m\mathbf{f} \quad (a \leq r \leq b) \quad (2.8)$$

Further, by substituting (2.1) to (2.3) and (2.6) to (2.8) into the boundary condition of each interface between media given below:

$$r=a \quad E_f^m = 0 \quad (2.9)$$

$$r=b \quad E_f^m = E_f^I + E_f^S \quad (2.10)$$

$$H_z^m = H_z^I + H_z^S \quad (2.11)$$

the amplitude coefficient b_m of scattered wave from tree trunk E_f^S was obtained as;

$$b_m = -\frac{U_m j^m (\mathbf{a}_m Z_r J_m(k_o b) - \mathbf{b}_m J_m'(k_o b))}{\left(\mathbf{a}_m Z_r H_m^{(2)}(k_o b) - \mathbf{b}_m H_m^{(2)'}(k_o b) \right)} \quad (2.12)$$

where

$$Z_r = \sqrt{\mathbf{m}_r / \mathbf{e}_r}$$

$$\mathbf{a}_m = N_m'(kb) J_m'(ka) - N_m'(ka) J_m'(kb)$$

$$\mathbf{b}_m = N_m(kb) J_m'(ka) - N_m'(ka) J_m(kb)$$

Finally, by substituting the amplitude coefficient b_m of (2.12) into (2.7), the scattered electric field is obtained.

In the same manner, fields of transverse magnetic (TM) mode that scattered from two layers of tree trunk could be derived (see Appendix A) and are obtained as below. Where the electric fields are

$$\text{Incident wave} \quad E_z^I = E_o^I \sum_{m=0}^{\infty} U_m J_m(k_o r) j^m \cos m\mathbf{f} \quad (r > b) \quad (2.13)$$

$$\text{Scattered wave} \quad E_z^S = E_o^I \sum_{m=0}^{\infty} b_m H_m^{(2)}(k_o r) \cos m\mathbf{f} \quad (r > b) \quad (2.14)$$

$$\text{Transmitted wave} \quad E_z^m = E_o^I \sum_{m=0}^{\infty} \{a_m J_m(kr) + a_m' N_m(kr)\} \cos m\mathbf{f} \quad (a \leq r \leq b) \quad (2.15)$$

and the magnetic fields are

$$H_f^I = \frac{k_o E_o^I}{j\omega m_o} \sum_{m=0}^{\infty} U_m J'_m(k_o r) j^m \cos m\mathbf{f} \quad (r > b) \quad (2.16)$$

$$H_f^S = \frac{k_o E_o^I}{j\omega m_o} \sum_{m=0}^{\infty} b_m H_m^{(2)'}(k_o r) \cos m\mathbf{f} \quad (r > b) \quad (2.17)$$

$$H_f^m = \frac{k E_o^I}{j\omega m} \sum_{m=0}^{\infty} \{a_m J'_m(kr) + a'_m N'_m(kr)\} \cos m\mathbf{f} \quad (a \leq r \leq b) \quad (2.18)$$

Finally, amplitude coefficient b_m for transverse magnetic mode is derived as

$$b_m = -\frac{U_m j^m \{a_m Z_r J'_m(k_o b) - b_m J_m(k_o b)\}}{a_m Z_r H_m^{(2)'}(k_o b) - b_m H_m^{(2)}(k_o b)} \quad (2.19)$$

where

$$a_m = J_m(ka)N_m(kb) - J_m(kb)N_m(ka)$$

$$b_m = J_m(ka)N'_m(kb) - J'_m(kb)N_m(ka)$$

To confirm the analysis result, the simulation of scattered wave from a pine tree trunk using Finite Difference Time Domain (FDTD) method is discussed in the next section.

2.3. Simulation

The JERS-1 SAR operated in horizontal (H) polarization on both transmits and receives. Hence horizontal polarization or transverse electric (TE) mode is considered in this study. Hence, electromagnetic field components are considered as $(E_x, E_y, 0)$ and $(0, 0, H_z)$.

Figure C.1 (in Appendix C) shows the position of field components in the finite-difference grid (unit of sample spacing). By referring this figure, the detail scattered electromagnetic fields E^S and H^S that are derived from Maxwell's equations are discussed in Appendix C, where the electromagnetic fields are shown in (2.20) to (2.22). In the derivation of these equation, Δt is time step, and Δx , Δy are sample spacing in x and y-axis, respectively. Here, the notation of Yee (Yee 1966) is used to replace $H^{(n+\frac{1}{2})\Delta t}$ as $H^{(n+\frac{1}{2})}$. Similarly, scattered

fields $\mathbf{E}^{S,t}(x, y)$ and $\mathbf{H}^{S,t}(x, y)$ are expressed as $\mathbf{E}^{S,n}(i, j)$ and $\mathbf{H}^{S,n}(i, j)$, where $t = n\Delta t$, $x = i\Delta x$ and $y = j\Delta y$. Sampling lead to the characteristic staggered finite-difference grid. In this grid, the electromagnetic field components are offset by $\Delta t/2$ in time and $\Delta x/2$ and $\Delta y/2$ in space. In the former, the field components are updated sequentially in time.

$$\begin{aligned}
E_x^{S,n}\left(i + \frac{1}{2}, j\right) &= \frac{1 - \mathbf{s}\left(i + \frac{1}{2}, j\right)\Delta t/2\mathbf{e}\left(i + \frac{1}{2}, j\right)}{1 + \mathbf{s}\left(i + \frac{1}{2}, j\right)\Delta t/2\mathbf{e}\left(i + \frac{1}{2}, j\right)} E_x^{S,n-1}\left(i + \frac{1}{2}, j\right) \\
&+ \frac{\Delta t/\mathbf{e}\left(i + \frac{1}{2}, j\right)}{1 + \mathbf{s}\left(i + \frac{1}{2}, j\right)\Delta t/2\mathbf{e}\left(i + \frac{1}{2}, j\right)} \frac{H_z^{S,n-\frac{1}{2}}\left(i + \frac{1}{2}, j + \frac{1}{2}\right) - H_z^{S,n-\frac{1}{2}}\left(i + \frac{1}{2}, j - \frac{1}{2}\right)}{\Delta y} \\
&- \frac{\mathbf{s}\left(i + \frac{1}{2}, j\right)\Delta t/2\mathbf{e}\left(i + \frac{1}{2}, j\right) - (\mathbf{e}\left(i + \frac{1}{2}, j\right) - \mathbf{e}_o)/\mathbf{e}\left(i + \frac{1}{2}, j\right)}{1 + \mathbf{s}\left(i + \frac{1}{2}, j\right)\Delta t/2\mathbf{e}\left(i + \frac{1}{2}, j\right)} E_x^{I,n-1}\left(i + \frac{1}{2}, j\right) \\
&- \frac{\mathbf{s}\left(i + \frac{1}{2}, j\right)\Delta t/2\mathbf{e}\left(i + \frac{1}{2}, j\right) + (\mathbf{e}\left(i + \frac{1}{2}, j\right) - \mathbf{e}_o)/\mathbf{e}\left(i + \frac{1}{2}, j\right)}{1 + \mathbf{s}\left(i + \frac{1}{2}, j\right)\Delta t/2\mathbf{e}\left(i + \frac{1}{2}, j\right)} E_x^{I,n}\left(i + \frac{1}{2}, j\right)
\end{aligned} \tag{2.20}$$

$$\begin{aligned}
E_y^{S,n}\left(i, j + \frac{1}{2}\right) &= \frac{1 - \mathbf{s}\left(i, j + \frac{1}{2}\right)\Delta t/2\mathbf{e}\left(i, j + \frac{1}{2}\right)}{1 + \mathbf{s}\left(i, j + \frac{1}{2}\right)\Delta t/2\mathbf{e}\left(i, j + \frac{1}{2}\right)} E_y^{S,n-1}\left(i, j + \frac{1}{2}\right) \\
&- \frac{\Delta t/\mathbf{e}\left(i, j + \frac{1}{2}\right)}{1 + \mathbf{s}\left(i, j + \frac{1}{2}\right)\Delta t/2\mathbf{e}\left(i, j + \frac{1}{2}\right)} \frac{H_z^{S,n-\frac{1}{2}}\left(i + \frac{1}{2}, j + \frac{1}{2}\right) - H_z^{S,n-\frac{1}{2}}\left(i - \frac{1}{2}, j + \frac{1}{2}\right)}{\Delta x} \\
&- \frac{\mathbf{s}\left(i, j + \frac{1}{2}\right)\Delta t/2\mathbf{e}\left(i, j + \frac{1}{2}\right) - (\mathbf{e}\left(i, j + \frac{1}{2}\right) - \mathbf{e}_o)/\mathbf{e}\left(i, j + \frac{1}{2}\right)}{1 + \mathbf{s}\left(i, j + \frac{1}{2}\right)\Delta t/2\mathbf{e}\left(i, j + \frac{1}{2}\right)} E_y^{I,n-1}\left(i, j + \frac{1}{2}\right) \\
&- \frac{\mathbf{s}\left(i, j + \frac{1}{2}\right)\Delta t/2\mathbf{e}\left(i, j + \frac{1}{2}\right) + (\mathbf{e}\left(i, j + \frac{1}{2}\right) - \mathbf{e}_o)/\mathbf{e}\left(i, j + \frac{1}{2}\right)}{1 + \mathbf{s}\left(i, j + \frac{1}{2}\right)\Delta t/2\mathbf{e}\left(i, j + \frac{1}{2}\right)} E_y^{I,n}\left(i, j + \frac{1}{2}\right)
\end{aligned} \tag{2.21}$$

$$\begin{aligned}
H_z^{S,n+\frac{1}{2}}\left(i + \frac{1}{2}, j + \frac{1}{2}\right) &= \\
&H_z^{S,n-\frac{1}{2}}\left(i + \frac{1}{2}, j + \frac{1}{2}\right) - \frac{\Delta t}{\mathbf{m}\left(i + \frac{1}{2}, j + \frac{1}{2}\right)\Delta x} \left(E_y^{S,n}\left(i + 1, j + \frac{1}{2}\right) - E_y^{S,n}\left(i, j + \frac{1}{2}\right)\right) \\
&+ \frac{\Delta t}{\mathbf{m}\left(i + \frac{1}{2}, j + \frac{1}{2}\right)\Delta y} \left(E_x^{S,n}\left(i + \frac{1}{2}, j + 1\right) - E_x^{S,n}\left(i + \frac{1}{2}, j\right)\right) \\
&- \frac{\mathbf{m}\left(i + \frac{1}{2}, j + \frac{1}{2}\right) - \mathbf{m}_o}{\mathbf{m}\left(i + \frac{1}{2}, j + \frac{1}{2}\right)} \left(H_z^{I,n+\frac{1}{2}}\left(i + \frac{1}{2}, j + \frac{1}{2}\right) - H_z^{I,n-\frac{1}{2}}\left(i + \frac{1}{2}, j + \frac{1}{2}\right)\right)
\end{aligned} \tag{2.22}$$

where $\mathbf{m}(i, j)$, $\mathbf{e}(i, j)$, $\mathbf{s}(i, j)$ are the characteristics of wave propagation media in simulation space. \mathbf{E}^s and \mathbf{H}^s are scattered electromagnetic fields that derived from Maxwell's equations. \mathbf{e}_o and \mathbf{m}_o are dielectric constant and permeability of free space, respectively. \mathbf{E}^i and \mathbf{H}^i are space functions of incident electromagnetic fields. In this research, horizontal polarization or transverse electric wave was considered. Consequently, in this simulation, electromagnetic field components were considered as $(E_x, E_y, 0)$ and $(0, 0, H_z)$.

When implementing the finite-difference scheme, boundary conditions must be treated in a special manner. Two different kinds of boundaries: the internal boundaries (*i.e.*, boundaries within the medium marked by a change in material properties) and the external boundaries (*i.e.*, the grid edges). The conditions at internal boundaries (*i.e.*, at the interfaces between different media) are usually satisfied implicitly. However, to ensure numerical stability, the material properties must be averaged for components on boundary. For transitions between similar materials, the averaging may be omitted. However, it is necessary at an interface between media with greatly different material properties (for example, at an air – skin interface) in order to maintain the stability. The finite-difference model is implemented in two-dimensions (2-D) as shown in figure 2.2. In this figure, simulation space is sampled into $INX \times INY$ grids. FDTD method can only simulate a finite space, but real scattering problems are often in the infinite formations. In this case, artificial external boundaries must be applied in the FDTD method. To prevent these artificial boundaries from reflecting electromagnetic waves, absorbing boundary conditions are used. In 1981, Gerrit Mur introduced simple absorbing boundary conditions to truncate FDTD meshes (Gerrit 1981). The second kind of Mur method was applied in this analysis, because it involves small calculation-memory size and its accuracy is assured (Uno 1998). In this study, for example, electric field in $i=1$ is determined as;

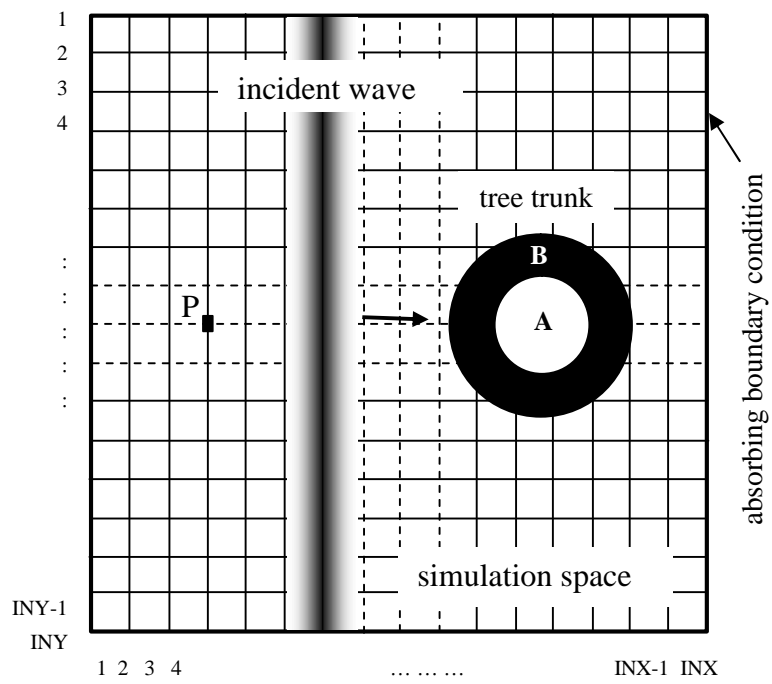


Figure 2.2. Simulation model.

$$\begin{aligned}
E_y^{S,n}(1, j) = & -E_y^{S,n-2}(2, j) + \frac{v\Delta t - \Delta x}{v\Delta t + \Delta x} \left\{ E_y^{S,n}(2, j) + E_y^{S,n-2}(1, j) \right\} \\
& + \frac{2\Delta x}{v\Delta t + \Delta x} \left\{ E_y^{S,n-1}(1, j) + E_y^{S,n-1}(2, j) \right\} + \frac{\Delta x (v\Delta t)^2}{2\Delta y^2 (v\Delta t + \Delta x)} \left\{ E_y^{S,n-1}(1, j+1) \right. \\
& \left. - 2E_y^{S,n-1}(1, j) + E_y^{S,n-1}(1, j-1) + E_y^{S,n-1}(2, j+1) - 2E_y^{S,n-1}(2, j) + E_y^{S,n-1}(2, j-1) \right\}
\end{aligned} \tag{2.23}$$

In the same manner, the other components of electric field in $i=INX$, $j=1$, and $j=INY$ can be derived, where \mathbf{n} is wave speed.

Figure 2.2 depicts the simulation model where A and B are heartwood and skin layer, respectively. This model was done in two-dimension, where each medium has infinite length in z-axis. This simulation space is divided into $INX \times INY$ grids (unit of cell size). Incident wave is a plane wave of intensity as that shown by Gaussian pulse, where the power spectrum of it is smooth and it is easy to sample. This pulse propagates from left to right of the simulation space in light speed. The Gaussian pulse is defined by function

$$p(t) = \begin{cases} e^{-a(t-t_0)^2}, & (0 \leq t \leq 2t_0) \\ 0, & otherwise \end{cases} \tag{2.24}$$

Where t is running time, t_0 is pulse width, and $\mathbf{a} = (4/t_0)^2$. Figure 2.3 (a) and (b) show Gaussian pulse with $t_0 = 9 \times 10^{-9}$ s and its spectrum, respectively.

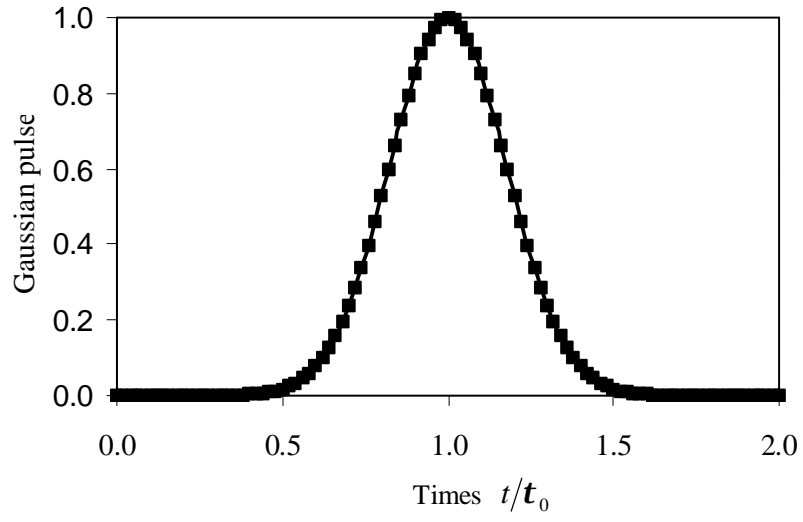
The geometry of incident wave is shown in figure 2.4, where plane wave propagates at angle \mathbf{f} with respect to x-axis. The propagation direction of the incident wave is determined as

$$\hat{\mathbf{r}}_0 = \hat{\mathbf{x}} \cos \mathbf{f} + \hat{\mathbf{y}} \sin \mathbf{f} \tag{2.25}$$

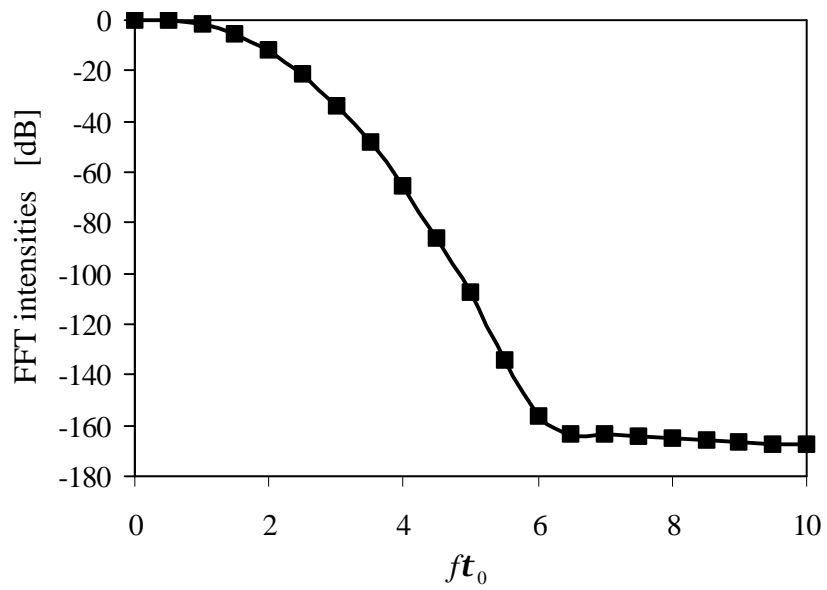
where $\hat{\mathbf{x}}$ and $\hat{\mathbf{y}}$ are unit vectors. Hence the incident electromagnetic fields are derived as

$$H_z^I(\mathbf{r}, t) = \frac{E_0}{Z_0} p(t + \hat{\mathbf{r}}_0 \cdot \mathbf{r}/c + t_0) \tag{2.26}$$

$$\mathbf{E}^I(\mathbf{r}, t) = E_0 (-\sin \mathbf{f} \hat{\mathbf{x}} + \cos \mathbf{f} \hat{\mathbf{y}}) p(t + \hat{\mathbf{r}}_0 \cdot \mathbf{r}/c + t_0) \tag{2.27}$$



(a) Gaussian pulse.



(b) Fast fourier transformed Gaussian pulse.

Figure 2.3. Pulse of incident wave.

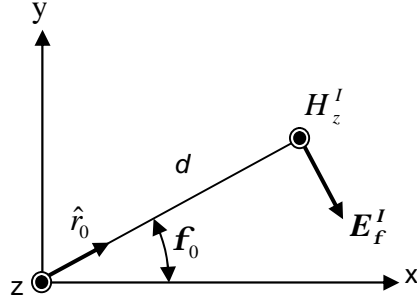


Figure 2.4. Geometry of incident wave

where c is speed of light. E_0 and Z_0 are initial intensity of incident electric field and wave impedance in free space, respectively. $p(t)$ is pulse function excited by Gaussian pulse (2.24). By substituting the components of electromagnetic fields in (2.26) and (2.27), and considering the Yee's notation, each component of electromagnetic fields of incident wave is acquired as follows;

$$H_z^{I,n+\frac{1}{2}}(i+\frac{1}{2}, j+\frac{1}{2}) = \frac{E_0}{Z_0} \cdot p\left((n+\frac{1}{2})\Delta t + \left\{ (i+\frac{1}{2})\Delta x \cos \mathbf{f} + (j+\frac{1}{2})\Delta y \sin \mathbf{f} \right\} / c - d/c\right) \quad (2.28)$$

$$E_x^{I,n}(i+\frac{1}{2}, j+1) = E_0 \cdot (-\sin \mathbf{f}) \cdot p\left(n\Delta t + \left\{ (i+\frac{1}{2})\Delta x \cos \mathbf{f} + (j+1)\Delta y \sin \mathbf{f} \right\} / c - d/c\right) \quad (2.29)$$

$$E_y^{I,n}(i+1, j+\frac{1}{2}) = E_0 \cdot \cos \mathbf{f} \cdot p\left(n\Delta t + \left\{ (i+1)\Delta x \cos \mathbf{f} + (j+\frac{1}{2})\Delta y \sin \mathbf{f} \right\} / c - d/c\right) \quad (2.30)$$

where $t_0 = -d/c$ means that the pulse head is at a distance d from the origin of coordinate at initial time ($t = 0$ s). For each time step, the value of excitation is added to the value calculated from the finite-difference scheme.

To arrange the time step and cell size, first, frequency f_{\max} must be decided from figure 2.3(b). Here f_{\max} is frequency in 120dB from maximum intensity of frequencies spectrum. It means that the accuracy of calculation is assured to six digits. By referring to this figure, $f_{\max} = 2.6$ GHz is obtained. By using empirical equation $\Delta x = \Delta y = v/10f_{\max}$ (Uno 1998), $\Delta x = \Delta y = 1.25 \times 10^{-2}$ m is obtained, where v is wave speed, in this study it is assumed

to be the same with wave speed in free space ($c = 3 \times 10^8 \text{ m/s}$). Finally, according to Courant condition (Uno 1998)

$$c\Delta t \leq 1/\sqrt{(1/\Delta x)^2 + (1/\Delta y)^2} \quad (2.31)$$

the time step Δt is obtained as $\Delta t = 2.5 \times 10^{-11} \text{ s}$. Finally, the two dimensional backscattering coefficient \mathbf{s}^o is defined as

$$\mathbf{s}^o = \frac{2pR}{l} \left(\frac{\langle |E_y^S|^2 \rangle}{\langle |E_y^I|^2 \rangle} \right)_{f=1.275 \text{ GHz}} \quad (2.32)$$

where E_y^I is observed or incident electric field intensity in frequency $f = 1.275 \text{ GHz}$ on the trunk surface. E_y^S is the intensity of electric field in observed point. l is effective surface of tree trunk for scattered wave, where it is assumed as pb . To simplify the analysis, the trunk number in targeted area is not considered and the obtained backscattering coefficient is considered as the average backscattering coefficient of total tree trunk in a unit area.

2.4. Results and discussion

In simulation space, see figure 2.2, infinite length of tree trunk is considered. This tree trunk is composed of two media; skin and heartwood. The radius of tree trunk b varies from 0 to 40 grids (or 0 to 0.5 m). The simulation space edges are surrounded by artificial absorbing boundary condition (Mur method). Incident wave is a plane wave of intensity as that shown by Gaussian pulse, which propagates from left to right of the simulation space in speed of light. Parameters of simulation are the simulation space grids $INX = INY = 300$, space-increments $\Delta x = \Delta y = 1.25 \times 10^{-2} \text{ m}$, time-increment $\Delta t = 2.5 \times 10^{-11} \text{ s}$, maximum intensity of initial electric field 100 V/m, and running time $t = 600\Delta t \text{ s}$. Figure 2.5 shows scattered wave from pine tree trunk with $t = 50\Delta t$ to $300\Delta t \text{ s}$. Additionally, figure 2.5 at $t = 300\Delta t \text{ s}$ shows

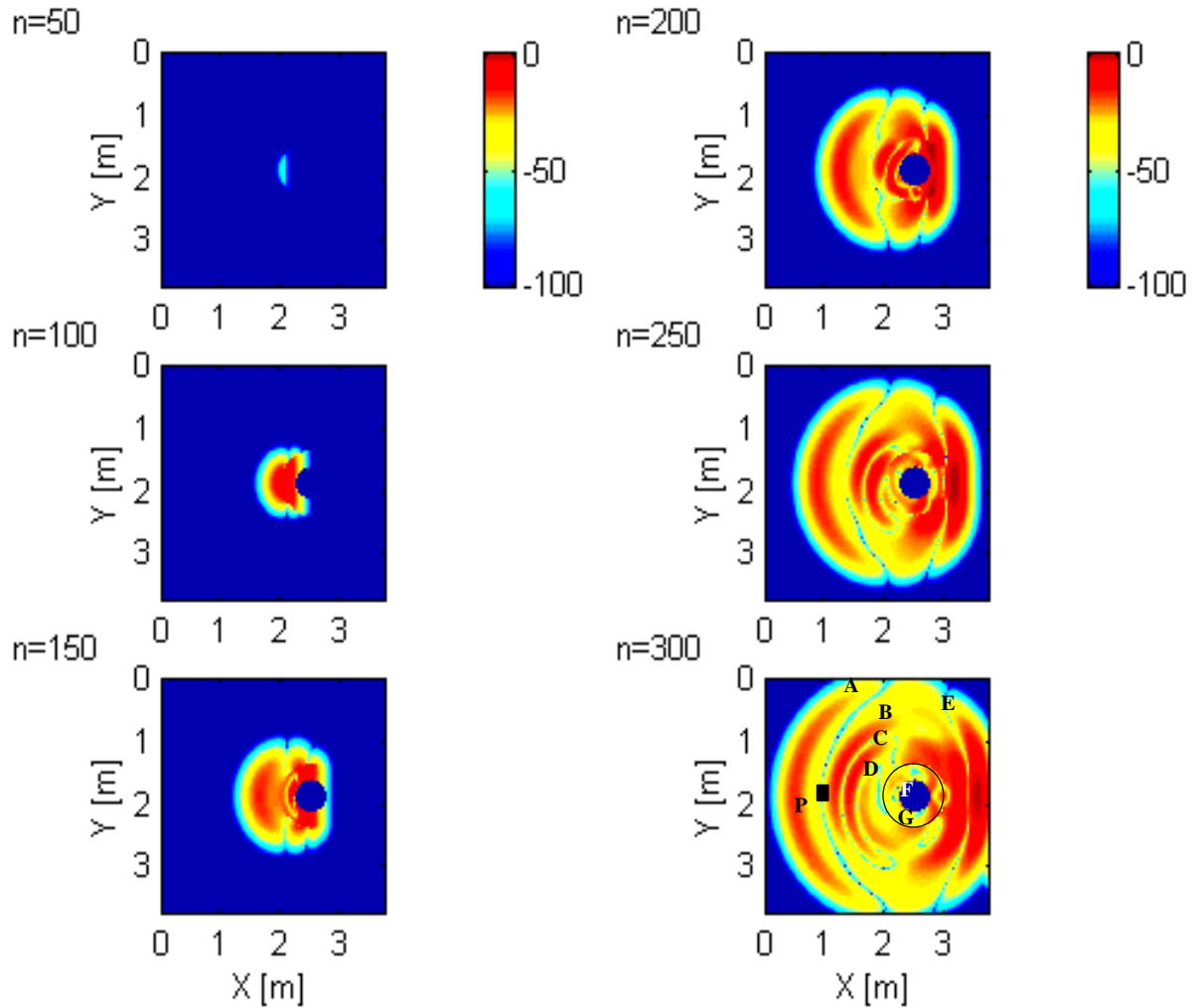


Figure 2.5. Scattered waves in simulation space from $t = 50\Delta t$ s to $300\Delta t$ s. A and B are scattered waves from skin and heartwood, C and D are scattered wave from trapped waves in skin layer, E is forwarded wave that occurred by clipping pulse that flows on the trunk surface and scattered to back of trunk, F and G are heartwood and skin, respectively. P is the observed point.

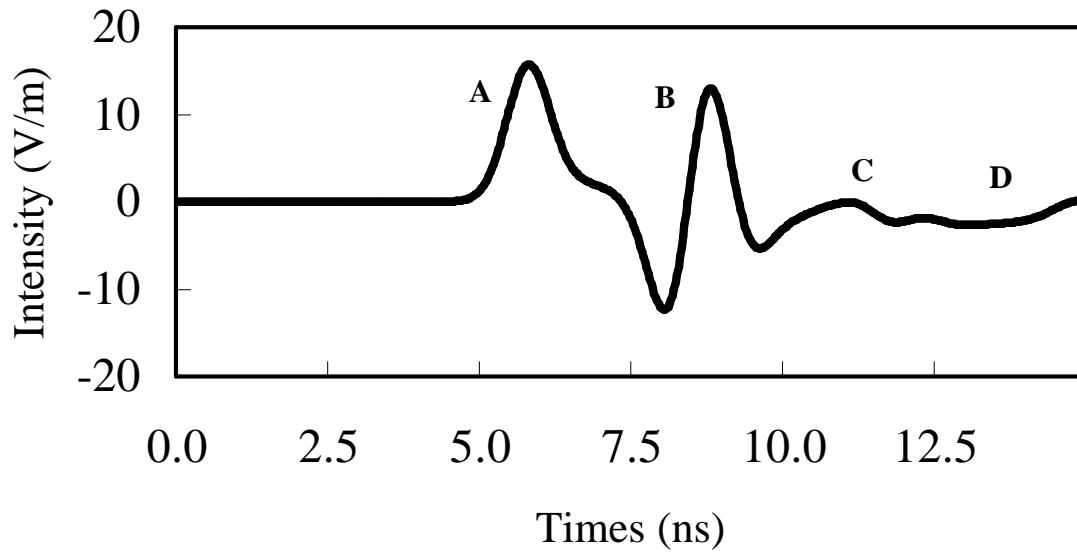


Figure 2.6. Scattered waves at observed point P: A and B, C and D are scattered pulse from skin and heartwood, and trapped wave in the skin layer, respectively.

details of scattered wave, where A and B are scattered waves from skin and heartwood, respectively. C and D are scattered wave from trapped waves in skin layer. E is forwarded wave. Then F and G are heartwood and skin, respectively. The observed point P is at 1.5 m from centre of tree trunk. This point is used to observe the intensities of scattered electromagnetic fields. In this study, the author observed only the horizontal polarisation component (transverse electric wave) or electric field E_y^s in backscattering direction ($f_o = 0^\circ$). The backscattered electric field is computed and is shown in figure 2.6. In this figure, A and B, C and D show scattered waves from skin and heartwood, and trapped wave in the skin layer, respectively. Further, fast Fourier transform is employed to obtain the electric field intensity of preferred frequency, in this case, frequency of Japanese Earth Resources Satellite (JERS-1) SAR, $f = 1.275$ GHz, is used. Finally, the backscattering coefficient is calculated using (2.32) and the results are shown in figure 2.7 (\square - simulation).

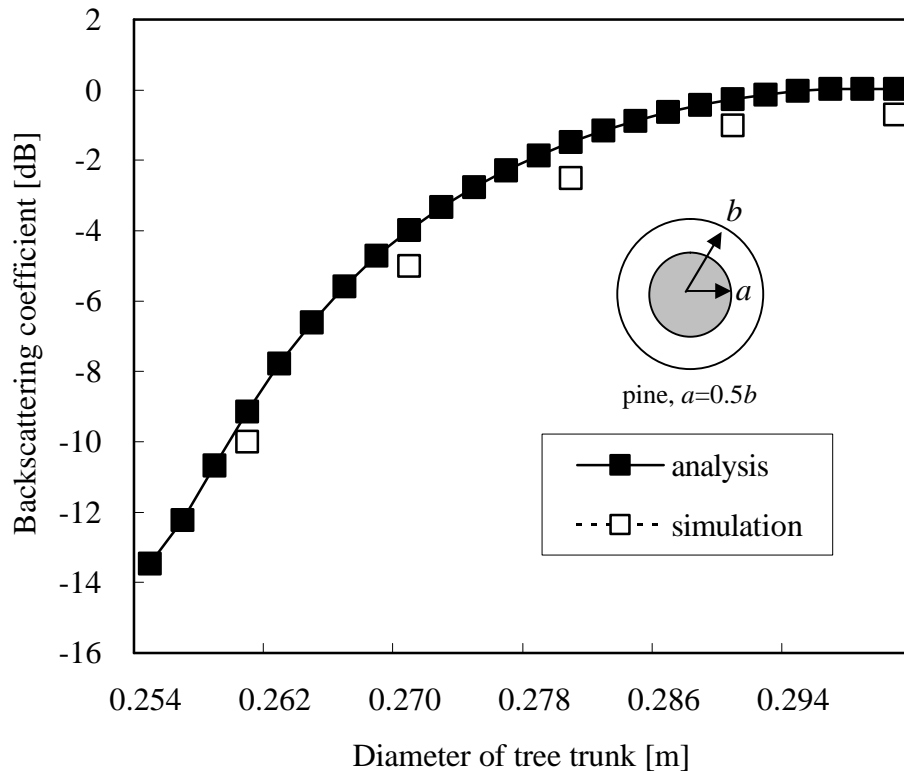


Figure 2.7. Relationship between tree trunk diameter and backscattering coefficient

In the analysis, direction of scattered wave is the same as observed point P or $f_o = 0^\circ$. Consequently, E_f^S in analysis is equivalent to E_y^S that calculated in the simulation. By substituting the parameters of JERS-1 SAR in the equations of analysis, the analysis results are obtained and are as shown in figure 2.7 (■ - analysis). The results compare well with simulation ones for a tree trunk (□ - simulation). However, a small error was found. It is considered that the error is generated by the Finite Difference Time Domain (FDTD) calculation error caused by calculation using the sampled space. In this analysis, the soil is assumed as perfectly conductor, hence figure 2.7 shows only pure backscattering coefficient of a tree trunk. In the next section, this result will be applied to estimate pine trunk diameter in the study area using JERS-1 SAR data.

2.5. Application

2.5.1. Study area

The study area is pine forest around Saguling lake, west Java, Indonesia (figure 2.8). The region has altitude ranging from 7m to 127m. Biomes of this area are pine forest, mixed vegetation area, settlement and paddy fields called *ladang* (dry paddy fields). The soil condition around the study area is wet. The ground data of the study area were collected in 1999 (Ketut 2001). The annual average rainfall of this area was 233 days, while the annual average temperature is 23°C.

2.5.2. Data processing

The JERS-1 SAR data was examined in order to estimate the diameters of pine tree trunk in the study area. The data (path 106, row 312) was acquired on 13 May 1997 during the

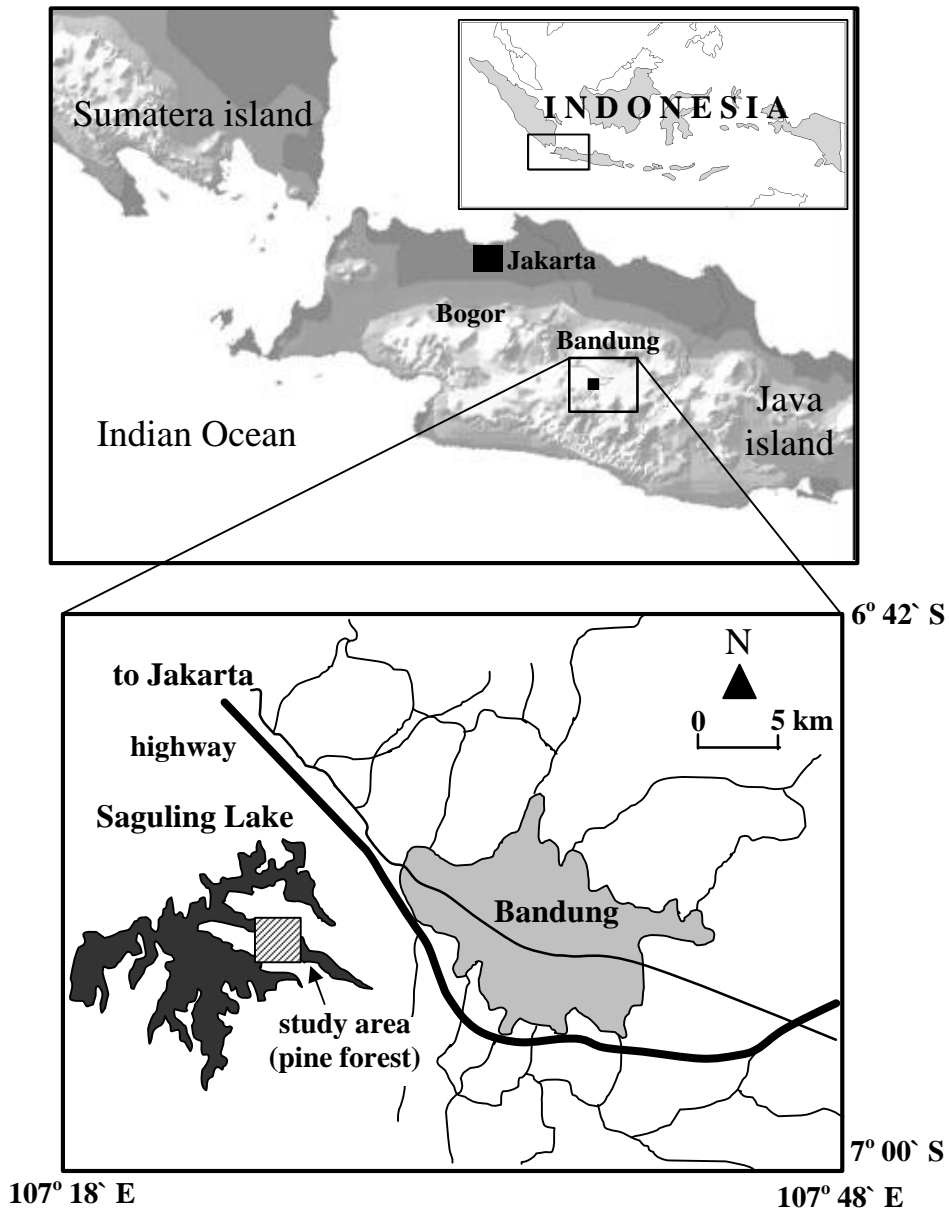


Figure 2.8. Map of the study area



Pine forest in the study area

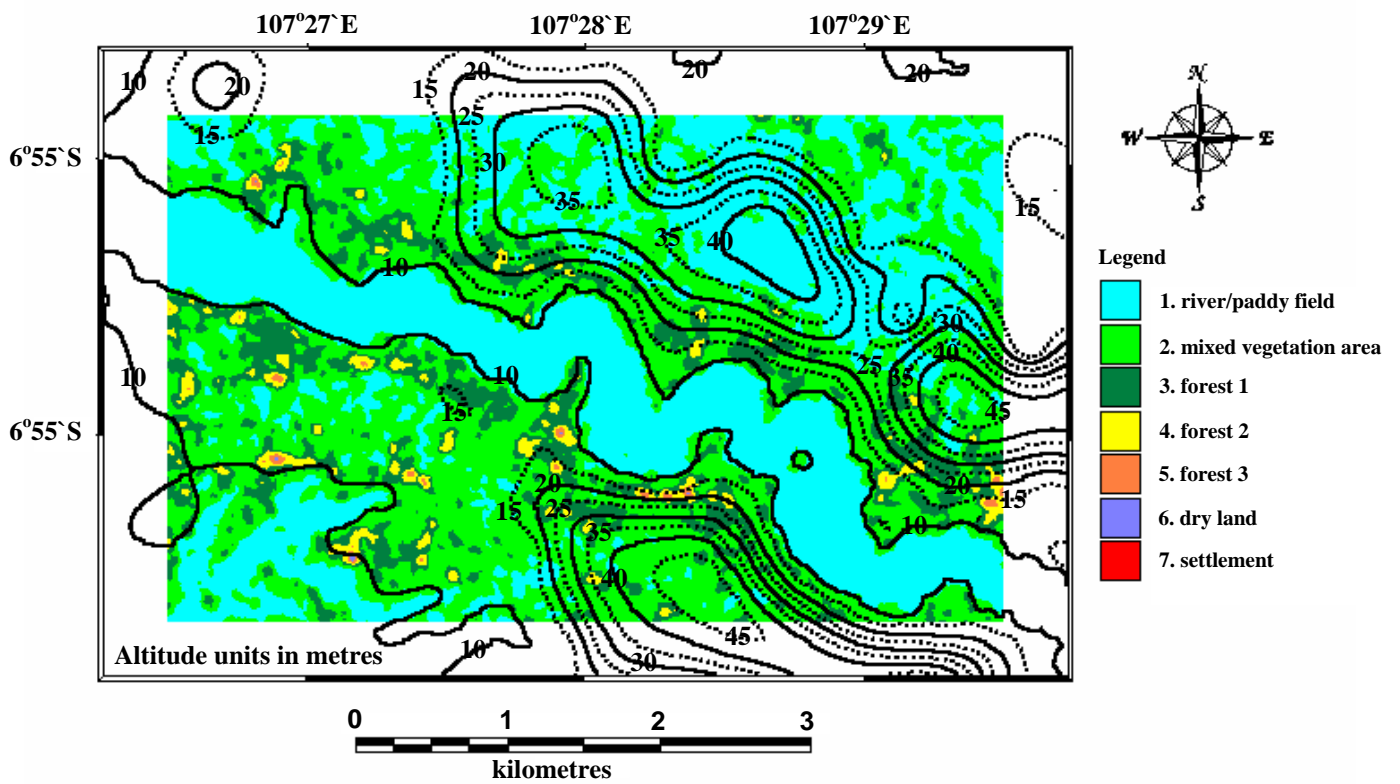


Figure 2.9. Photograph of pine forest in the study area and the supervised classification results of JERS-1 SAR data (path 106, row 312, 13 May 1997).

Table 2.1. Classification and estimation results

Class names	Backscattering coefficient σ^o (dB)	Diameter of tree trunk (m)	Standard deviation (m)
forest 1	-10	0.260	0.0025
forest 2	-8	0.265	0.0025
forest 3	-5	0.270	0.0025

dry season in the study area. This image was processed at level 2.1 or standard geocoded data and was resampled to the Universal Transverse Mercator (UTM) projection by the Earth Observation Research Centre (EORC) of the National Space Development Agency (NASDA) of Japan. Firstly, a 3x3 median filter was employed and secondly, process used a 5x5 average filter to reduce inherent speckle noise (Sunar *et al.* 1998). At the same time, the data was also referenced to the UTM co-ordinate system, through a polynomial rectification using 30 ground control points collected from topographic maps scale of 1:25.000 (BAKOSURTANAL 1990). This procedure yielded a geometric accuracy of 0.1 pixels. Then the spatial resolution of SAR data was resampled to 12.5m.

A supervised classification was performed to classify the satellite data into seven classes. The topographic maps and ground data were used to select training sites (Ketut 2001), i.e. river and paddy field, bush, forest 1, forest 2, forest 3, mixed forest, and settlement (figure 2.9). By supervised classification, the average pixel intensity I of each class was obtained. These values were substituted in the equation $\sigma^o = 20 \log I - 68.2$ dB (Shimada 1998) to obtain backscattering coefficients. By plotting the results on figure 2.7, the average diameter of each class was obtained (see table 2.1). The estimation result shows the diameter of pine in

the study area was between 0.26m and 0.27m and has standard deviation 0.0025m. A sampling of 10 locations yielded similar results to the ground data that collected in 1999 (Ketut 2001).

2.6. Conclusions

A simple numerical analysis was conducted to analyse the relationship between the backscattering coefficients S^o and diameter of pine tree trunk. The analysis results were confirmed by simulation using Finite Difference Time Domain (FDTD) method. These results are in good agreement. A variation of this analysis, it could be applied to estimate diameter of tropical tree trunk from Synthetic Aperture Radar (SAR) data, which this information is very important to estimate the forest volumes or biomass effectively and accurately. These results succeeded in estimating tree trunk diameter of pine (*Pinus merkusii*) that is widely distributed in the west Java forest, Indonesia from JERS-1 SAR data.

While this study focused on single site in Indonesia, it is reasonable to expect that this method or variations should be successful in estimating tree trunk diameters in similar forest regions of the world using SAR data.

References

1. BAKOSURTANAL, 1990, Topographic maps; 1209-223, 1209-241, 1209-242. Indonesian National Coordination Agency for Surveys and Mapping, 1st edition (Cibinong: Bakosurtanal).
2. COPPEN, J.J.W., GAY, C., JAMES, D.J., ROBINSON, J.M. and SUPRIANA, N., 1993, Variability in xylem resin composition amongst natural populations of Indonesian *Pinus merkusii*. *Phytochemistry*, 33, 129-136.
3. DAVID, P., STELLA, E.B., STEPHEN, J.M., 1997, Terrain influences on SAR backscatter around Mt. Taranaki, New Zealand. *IEEE Transactions on Geoscience and Remote Sensing*, 35, 924-932.
4. FAO, 1995, Flavours and fragrances of plant origin. Food and Agriculture Organisation (FAO), United Nations, Chapter 8, 1st edition (Rome: FAO-UN).
5. GERRIT MUR, 1981, Absorbing boundary conditions for the finite-difference approximation of the time-domain electromagnetic-field equation. *IEEE Transactions on Electromagnetic Compatibility*, 23, 377-382.
6. KETUT WIKANTIKA, 2001, Spectral and textural aspects of multisensor and multitemporal satellite data for land use / land cover mapping in a tropical area. Ph.D Dissertation, Chiba University, January 2001 (Chiba: Chiba University).
7. SHIMADA, M., 1998, User's guide to NASDA's SAR products. Earth Observation Research Centre, National Space Development Agency (NASDA), 2nd edition (Tokyo: NASDA).
8. SUNAR, F., TABERNER, M., MAKTAV, D., KAYA, S., MUSAOGLU, M., and YAGIZ, E., 1998, The use of multi temporal radar data in agriculture monitoring: a case study in Kyocegiz-Dalaman ecosystem, Turkey. *International Archives of Photogrammetry and Remote Sensing*, 22, 559-565.

9. TETUKO S.S., J., R. TATEISHI, K. WIKANTIKA, 2001, A method to estimate tree trunk diameter and its application to discriminate Java-Indonesia tropical forests. *International Journal of Remote Sensing*, 22, 177-183.
10. UNO TORU, 1998, Finite difference time domain method for electromagnetic field and antenna analyses. 1st edition (Tokyo: Corona).
11. YEE, K. S., 1966, Numerical solution of initial boundary value problems involving Maxwell's equations in isotropic media. *IEEE Transactions on Antennas Propagation*, 14, 302-307.

